Thermal Response of Langmuir-Blodgett Films of Dipalmitoylphosphatidylcholine Studied by Atomic Force Microscopy and Force Spectroscopy

Gerard Oncins,* Laura Picas,† Jordi Hernández-Borrell,† Sergi Garcia-Manyes,* and Fausto Sanz*
*Department of Physical Chemistry, Chemistry Faculty, University of Barcelona and Institut de Bioenginyeria de Catalunya, Barcelona, Spain; and †Department of Physical Chemistry, Pharmacy Faculty, University of Barcelona, Barcelona, Spain

ABSTRACT The topographic evolution of supported dipalmitoylphosphatidylcholine (DPPC) monolayers with temperature has been followed by atomic force microscopy in liquid environment, revealing the presence of only one phase transition event at ~46°C. This finding is a direct experimental proof that the two phase transitions observed in the corresponding bilayers correspond to the individual phase transition of the two leaflets composing the bilayer. The transition temperature and its dependency on the measuring medium (liquid saline solution or air) is discussed in terms of changes in van der Waals, hydration, and hydrophobic/hydrophilic interactions, and it is directly compared with the transition temperatures observed in the related bilayers under the same experimental conditions. Force spectroscopy allows us to probe the nanomechanical properties of such monolayers as a function of temperature. These measurements show that the force needed to puncture the monolayers is highly dependent on the temperature and on the phospholipid phase, ranging from 120 ± 4 pN at room temperature (liquid condensed phase) to 49 ± 2 pN at 65°C (liquid expanded phase), which represents a two orders-of-magnitude decrease respective to the forces needed to puncture DPPC bilayers. The topographic study of the monolayers in air around the transition temperature revealed the presence of boundary domains in the monolayer surface forming 120° angles between them, thus suggesting that the cooling process from the liquid-expanded to the liquid-condensed phase follows a nucleation and growth mechanism.

INTRODUCTION

Physicochemical properties of biomembranes have been a matter of extensive research along the years. The elucidation of the transport processes across these structures as well as the understanding of the cell surface functionality has become common ground for interdisciplinary studies concerning physics, chemistry, and biology. Although biomembranes are known to be heterogeneous in composition, phospholipid molecules are the predominant species. Therefore, the study of the physicochemical properties of phospholipid assemblies, both in the bilayer and monolayer forms, was shown to be crucial to the comprehension of model membranes.

Understanding the effect of mechanical stress on biological membranes is of fundamental importance since cells are known to naturally perform their function under the effect of a complex combination of forces (1). Indeed, the chemical composition of such membranes is, in the main, responsible for determining their architecture, while guaranteeing the cell mechanical stability (2). To decipher the partial contribution of the membrane onto the overall cell mechanical integrity, several studies have been focused on the study of lipid bilayers, since they correctly mimic cell membranes up to an extent (3). So far, lipid bilayers have been extensively studied from a mechanical point of view. In the mesoscopic range, calorimetric experiments (4) and the development of techniques to manipulate giant vesicles have rendered experimental quantitative values for membrane curvature modulus and hydrodynamic shear viscosity (5–8). Down to the nanoscale, atomic force microscopy (AFM) and related techniques have become really useful so as to characterize the topography of supported planar bilayers (SPBs), that is, bilayers deposited on a flat surface, typically SiO_2, highly oriented pyrolitic graphite or mica (9–12) with nanometer resolution.

Besides, AFM in its force-spectroscopy mode offers the possibility to extremely locally compress a supported bilayer with an AFM probe while precisely controlling the applied force with pN resolution. The analysis of the probe deflection during the compression process allows studying the elastic and plastic behavior of the bilayer. Several works have observed that the AFM probe can puncture the bilayer (13–15) provided that a certain threshold force is applied, giving rise to a discontinuity or jump in the force-extension curve. The force at which the bilayer breaks (yield threshold force, F_y) can be considered as a fingerprint of the phospholipid phase, as it is intimately related with the intermolecular forces arisen among the phospholipid molecules, the substrate, and the surrounding medium.

Along these lines, we recently reported (16) that an increase of the ionic strength in the measuring medium resulted in a higher F_y value due to a reduction of the area/lipid ratio as predicted by molecular dynamics calculations (17), thus

Submitted April 26, 2007, and accepted for publication June 15, 2007.

Address reprint requests to F. Sanz, E-mail: fsanz@ub.edu; or to S. Garcia-Manyes, E-mail: sergi@biology.columbia.edu.

S. Garcia-Manyes's present address is Dept. of Biological Sciences, Columbia University, 1212 Amsterdam Ave., New York, NY 10027.

Editor: Peter Tieleman.

0006-3495/07/10/2713/13 $2.00

doi: 10.1529/biophysj.107.110916

highlighting the key role of electrostatic and van der Waals interactions in the bilayer compactness. Moreover, the interaction of the solvent with the phosphocholine polar heads and its key role in the overall bilayer stability has also been explored.

In a previous work, the evolution of such F_y value has been related to the changes in the topographic evolution of 1,2-dimyristoyl-*sn*-glycero-3-phosphocholine (DMPC) and dipalmitoylphosphatidylcholine (DPPC) SPBs (18). Previous differential scanning calorimetry experiments on DPPC liposomes established that there is a main transition between two lamellar phases while raising the temperature, the solid-crystalline (L_β) and the liquid-crystalline (L_α) state, which are characterized by a quasi-hexagonal array packing (solid) and a higher molecular motion (liquid), respectively (19). The phase transition of DPPC SPBs on mica has also been topographically followed by means of variable temperature AFM (20), yielding two consecutive transitions. It was proposed that the first observed phase transition could correspond to the main L_β-L_α transition and that the second one could be ascribed to a further transition occurring at high temperatures yielding to a highly disordered fluid phase. By contrast, further studies suggested that the two transitions could correspond to the individual melting of the DPPC leaflets that compose the bilayer (21). The low temperature transition was related to the melting of the leaflet that is far from the surface (distal leaflet), less stable than the leaflet in contact with the mica surface (proximal leaflet). Force spectroscopy experiments on DPPC SPBs have been directly related to the bilayer topographical changes as the temperature is changed (18). While in the L_β solid phase F_y decreases steadily as temperature increases reaching a minimum around transition temperature (T_M), in the L_α liquid phase F_y tends to plateau at a value slightly higher than that measured at T_M (18).These experiments concluded that F_y is an excellent experimental parameter to unambiguously characterize phospholipid phase transitions at the nanometer scale.

The nature of the two consecutive phase transitions observed in the bilayers could be elucidated by reproducing the same experiment with the respective monolayers. Furthermore, studying the thermal and mechanical response of single monolayers at the nanometer scale would help to shed light not only onto the phase transition phenomena, but also onto the more general study of the interactions arising between the involved interfaces (i.e., the surface, the monolayer and the liquid environment) and also between well-defined neighboring molecules. All these interactions are much more complex in the bilayer case, as curvature and asymmetry issues have to be taken into account.

DPPC monolayers have been extensively studied by using several methods such as light scattering (22–24) and spectroscopic techniques (25,26). The use of fluorescent lipid analogs that dissolve preferentially in the liquid-expanded (LE) phase permitted the morphological study of Langmuir monolayers while being compressed in the air-water interface (27). The shapes of the domains are characteristic for each pressure and therefore representative of the aggregation state of the DPPC monolayer. Similarly, by depositing the monolayer at the desired surface pressure onto a solid surface, AFM enables not only to visualize but also to gain insight into the nanostructure of the DPPC monolayer (28–32). Interestingly, DPPC is one of the major constituents of the pulmonary surfactant, a coating with extremely demanding mechanical properties and where the air-water interface plays a biologically relevant role.

The aim of this work is twofold. On the one hand, we aim to get further insight into the understanding of the physics underlying the two phase transitions described for SPBs. In brief, we are interested in elucidating whether the two consecutive phase transitions measured in variable temperature AFM experiments involve the separate melting of each of the two lipid leaflets composing the bilayer or if, on the contrary, two cooperative and consecutive phase transitions take place: the first one corresponding to the transition from the solid phase to liquid phase and the second one corresponding to the transition from liquid phase to liquid-disordered phase. On the other hand, we aim to characterize the nanomechanical properties of Langmuir-Blodgett phospholipid monolayers using force spectroscopy. In particular, we aim to correlate the mechanical properties of such monolayers with their thermodynamics phase as a function of temperature. These experiments serve as the ideal platform to compare the mechanical properties of bilayers and monolayers under the same experimental conditions, and to test the additivity of the process. Last but not least, we endeavor to topographically characterize the reversible nucleation and growth processes during the first stages of phase formation, which is a direct signature of molecular reorganization involved during the main phase transition.

MATERIALS AND METHODS

Sample preparation

The lipid (Avanti Polar Lipids, Alabaster, AL) was dissolved in chloroform-methanol (3:1, v/v) to a final concentration of 1 mg/mL^{-1}. The preparation of the Langmuir-Blodgett (LB) films of DPPC was performed in a 312 DMC Langmuir-Blodgett trough manufactured by NIMA Technology (Coventry, England). The trough was placed onto a vibration-isolated table (Newport, Irvine, CA) and enclosed in an environmental chamber. The subphase (150 mM NaCl + 20 mM $MgCl_2$, pH ~7.4 with 10 mM HEPES/NaOH) was filtered with a Kitasato University system (Tokyo, Japan; 450-nm pore diameter) before use. The same buffer solution was used as liquid medium for imaging and force spectroscopy measurements. The resolution of surface pressure measurement was ± 0.1 mN/m^{-1}. In all experiments, the temperature was maintained at 24.0 $\pm$ 0.2°C by an external circulating water bath. Before each experiment, the trough was washed with chloroform and rinsed thoroughly with purified water. The cleanliness of the trough and subphase was ensured before each run by cycling the full range of the trough area and aspirating the air-water surface while at the minimal surface area, to zero surface pressure.

The corresponding aliquots of lipid were spread, drop by drop, onto subphase solution with a microsyringe Hamilton (Reno, NV). A period of

15 min was required to allow the solvent to evaporate before the experiment was started. The compression barrier speed to the final surface pressure was 5 $cm^2\ min^{-1}$. LB films were transferred onto freshly cleaved mica, lifting the substrate at a constant rate of 1 mm/min^{-1}. The transfer ratios were evaluated and were near the unity, indicating that the mica was practically covered with the monolayer.

Temperature-controlled AFM imaging

AFM experiments were performed with a Multimode microscope (Digital Instruments, Santa Barbara, CA) controlled by a Nanoscope IV electronics (Digital Instruments, Santa Barbara, CA). Due to the softness of the monolayers, images were acquired in tapping mode (TM-AFM). V-shaped Si_3N_4 cantilevers (OMCL TR400PSA, Olympus, Japan) with a nominal spring constant of 0.08 N/m were used in liquid operation, while beam-shaped silicon oxide tapping tips (37th series B cantilever, MikroMasch, Portland, OR) with a nominal spring constant of 0.3 N/m were used in air. Images were acquired at minimum vertical force, that is, maximizing amplitude setpoint value while maintaining vibration amplitude as low as possible. Variable temperature experiments were performed attaching a temperature controller stage (Digital Instruments, Santa Barbara, CA) to the piezo-scanner. This device consists of a heating element placed below the magnetic sample holder and maintained at a fixed temperature (range: from room temperature up to 250°C, resolution: 0.1°C, accuracy: 3%, temperature drift: ±0.25°C). A water-ethanol fluid circuit refrigerates the piezo-scanner. It is very important to note that the heating element temperature is lower than the temperature of the sample surface; to operate in liquid environment, it is necessary to glue the mica surface to a Teflon disk that is glued to a metallic sample holder. The difference between the controller temperature and the real temperature of the sample surface can be as much as 25%, depending on the thickness of the Teflon and the epoxy glue. As a consequence, it is mandatory to calibrate sample holders individually before performing the measurements. To do that, a clean mica sheet is glued on the sample holder and a buffer droplet is spread on the surface as in a real experiment. Then, mica surface temperature is measured by a thermocouple (thermocouple thermometer model No. EW-91100-20 DigiSense; Cole Palmer, Foster City, CA. Resolution: 0.1°C, accuracy: ±0.25%, provided with Omega Precision Fine Wire Thermocouples; Omega Engineering, Stamford, CT) mounted in direct contact with the mica and a temperature ramp is performed to obtain the temperature factor between the controller temperature and the mica surface temperature. Upon imaging, temperature was varied from room temperature up to 80°C. Before acquiring every image, we waited 5 min to reach the equilibrium temperature of the system, although in ~1 min, temperature remained stable. After capturing an image, the tip was lifted 30 μm from the surface and the sample was heated to the next temperature.

Roughness measurements

Roughness can be expressed in several ways, with the mean roughness (R_a) and the root mean-square (R_q) being the most representative ones,

$$R_a = \frac{1}{N}\sum_{i=1}^{N}|Z_i - Z_{ave}|, \quad (1)$$

where N is the total number of points within the given area, Z_i is the pixel height value in the z axis, and Z_{ave} is the average of all Z_i values within the given area. R_q can be expressed as

$$R_q = \sqrt{\left(\frac{1}{N}\sum_{i=1}^{N}Z_i^2\right)}. \quad (2)$$

The tendency of R_a and R_q as temperature increased is similar. Then, and for the sake of simplicity, only R_q measurements will be discussed; but both values (R_a and R_q) are presented later in Fig. 2.

Force spectroscopy

Force spectroscopy measurements in liquid media were performed using V-shaped Si_3N_4 tips (OMCL TR400PSA, Olympus, Japan) with a nominal spring constant of 0.08 N/m. However, individual spring constants were calibrated using the thermal noise routine (33) implemented in a MFP-1D atomic force microscope (Asylum Research, Santa Barbara, CA). Typically 150–200 force plots were recorded at each temperature and they were performed maintaining the laser spot in the same position on the cantilever to keep constant the corresponding photodetector sensitivity (V/nm), which was calculated for each temperature (34). All spectroscopy experiments were performed at a constant cantilever linear velocity of 0.5 μm/s to avoid any velocity-dependent effect. Tip radius was individually measured by imaging a faceted silicon grating (Ultrasharp model No. TGG01, silicon oxide 3 μm pitch; MikroMasch, Portland, OR), obtaining values ranging from 15 to 35 nm. Applied vertical forces (F) are given by $F = k_c \times \Delta$, where Δ is the cantilever deflection and k_c is the cantilever spring constant. The surface deformation is given as penetration (δ) evaluated as $\delta = z - \Delta$, where z represents the piezo-scanner displacement. X, Y, and Z-piezo motion was calibrated with a DI silicon oxide grid (model No. STR10-1800P), 180 nm deep, 10 μm pitch (Digital Instruments, Santa Barbara; CA).

RESULTS AND DISCUSSION

LC-LE phase transition

DPPC monolayers were transferred to a mica surface at a surface pressure of 30 mN/m, which is considered a biologically relevant surface pressure (35). To ensure the correct transfer onto the mica substrate, a freshly prepared sample was scratched with the AFM tip and a vertical distance of ~2 nm between the top of the layer and the bottom of the trench was obtained as it is shown in the supporting information. Although the height measurement was acquired in TM-AFM (contact mode was too aggressive for this monolayer), its thickness corresponds reasonably well with values elsewhere reported for DPPC (36,37).

To investigate the topographic changes that DPPC monolayers undergo because of temperature changes, Fig. 1 shows a series of TM-AFM monolayer surface images in liquid environment as temperature is raised from 33.1°C up to 55.3°C, which corresponds to the temperature interval at which the phase transition of DPPC bilayers is expected. Fig. 1, *a* and *b*, were acquired at 33.1°C and 43.6°C, respectively, and the topographic images reveal a homogeneous and flat DPPC monolayer. As a reference, the T_M measured for DPPC liposomes in solution is 41.5°C (38). Upon raising the temperature up to 45.4°C, the topography undergoes a sudden roughness increase that can be already appreciated by visual inspection of Fig. 1 *c*. The same topographic features are still observed at 47.8°C (Fig. 1 *d*). This topographic change is likely to correspond to the monolayer phase transition, which will be further investigated in a roughness analysis of the surface. With increasing temperature, the topography undergoes a new change, as can be observed in Fig. 1, *e* and *f*, acquired at 51.6°C and 55.3°C, respectively. In both images the sample appears to be totally flat again.

A monolayer phase transition implies a range of temperatures in which both LC and LE phases coexist. As LC and

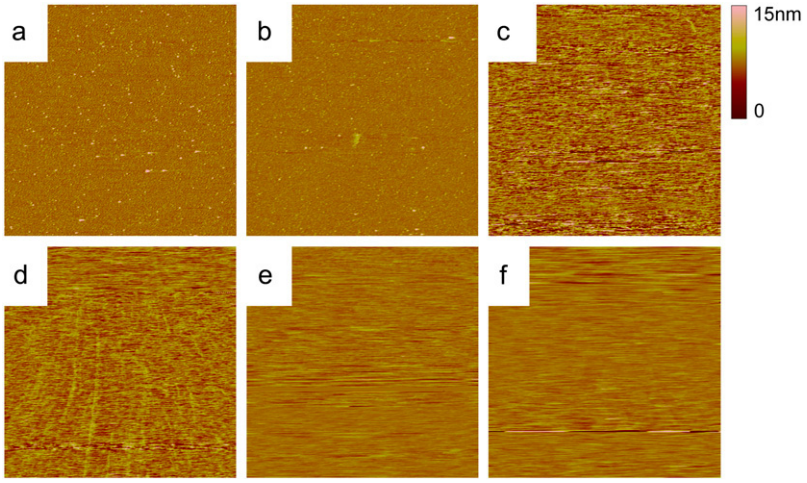

FIGURE 1 5×5 μm AFM tapping images of a DPPC monolayer extracted at 30 mN/m and imaged in buffer solution. The images were obtained at variable temperature; (*a*) 33.1°C; (*b*) 43.6°C; (*c*) 45.4°C; (*d*) 47.8°C; (*e*) 51.6°C; and (*f*) 55.3°C. Images *a* and *b* correspond to the LC phase, while images *c* and *d* represent the phase transition. Images *e* and *f* correspond to the LE phase.

LE phases have different thickness values (39,40), the images involving the coexistence of two phases should show a sharp increase in roughness with respect to the images in which the monolayer remains in a single phase (either LC or LE phase). The roughness analysis of the images shown in Fig. 1 is depicted in Fig. 2 *a* in terms of R_q and R_a. At 33.1°C, R_q was 0.9 nm and this value decreased down to 0.6 nm at 43.6°C. This roughness decrease is consistent with an increase in phospholipid mobility. Indeed, fluorescence recovery after photobleaching experiments on egg-phosphocholine monolayers and bilayers (41) showed that phospholipid diffusion coefficient increases with temperature and that it also depends strongly both on the nature of the phospholipid polar head and the surface pressure of the monolayer (42,43), mainly due to different electrostatic interactions between polar heads. Therefore, the decrease in roughness as temperature approaches T_M can be easily attributed to the promotion of the DPPC diffusion. Recent bending rigidity studies on DPPC giant liposomes showed that the value of this mechanical magnitude decreases steeply in the range of temperatures from the so-called pretransition temperature to T_M (5), according to the predictions of a previous model (44). These results were interpreted as the bilayer softening due to hydrocarbon chains melting, a process that increases the homogeneity of the monolayer and, consequently, its surface smoothness (which would give rise to a decrease in roughness value).

As it is shown in Fig. 2 *a*, between 43.6°C and 51.6°C, R_q increased by a factor of 3 (from ~0.7 nm up to ~2.5 nm). This observation may be accounted for as a result of the coexistence of the LC-LE phases, therefore implying a difference in the respective thickness value for the monolayer in both LC and LE phases. The in situ AFM variable temperature experiments performed by Feng et al. showed that the height decrease due to the transition of each of the leaflets present in a DPPC bilayer is 0.37 nm (45) and Charrier et al. (46) reported values of 0.4–0.7 nm for DMPC bilayers. This height change is attributed to the increase of the tilting angle of the DPPC molecule respective to the surface perpendicular as transition takes place (a 25° angle tilting was calculated for LC phase (47). The phase transition also implies the hydration of the polar heads as the molecules fluidize (40). Hence, the coexistence of two phases with different tilting angle (LC and LE phase) during the transition are very likely to be responsible for the increase in roughness observed between 43.6°C and 51.6°C in the case of the DPPC monolayers under study. At higher temperatures roughness decreases again, which is consistent with the higher mobility of the LE phase respect to the LC phase. Therefore, roughness measurements seem to be a reliable experimental signature of the processes (phase transition) that the surface undergoes at the nanometric scale.

Four independent sets of experiments such as those shown in Fig. 1 were performed, confirming that DPPC monolayers only undergo one phase transition in contrast with the two transitions observed for DPPC bilayers in previous works. The transition temperature range is reproducible from sample to sample, being always observed between 43 and 52°C. One phase transition in monolayers directly supports the hypothesis about the individual melting of the two DPPC leaflets being responsible for the two transitions observed in bilayers. The other suggested possibility is that two consecutive phase transitions, each one involving the whole bilayer, would probably have also led to two transitions in the case of the monolayer.

Several transition temperatures were reported in the past for DPPC bilayers under different conditions. Values of 42.4°C and 44.8°C for SPBs adsorbed onto mica flakes were obtained by means of differential scanning calorimetry (31), both transitions being above DPPC liposomes T_M (41.5°C), and were attributed to the individual melting of the two DPPC leaflets. The higher transition temperatures of SPBs with respect to the nonsupported liposomes were interpreted as a stabilizing effect due to the electrostatic interactions

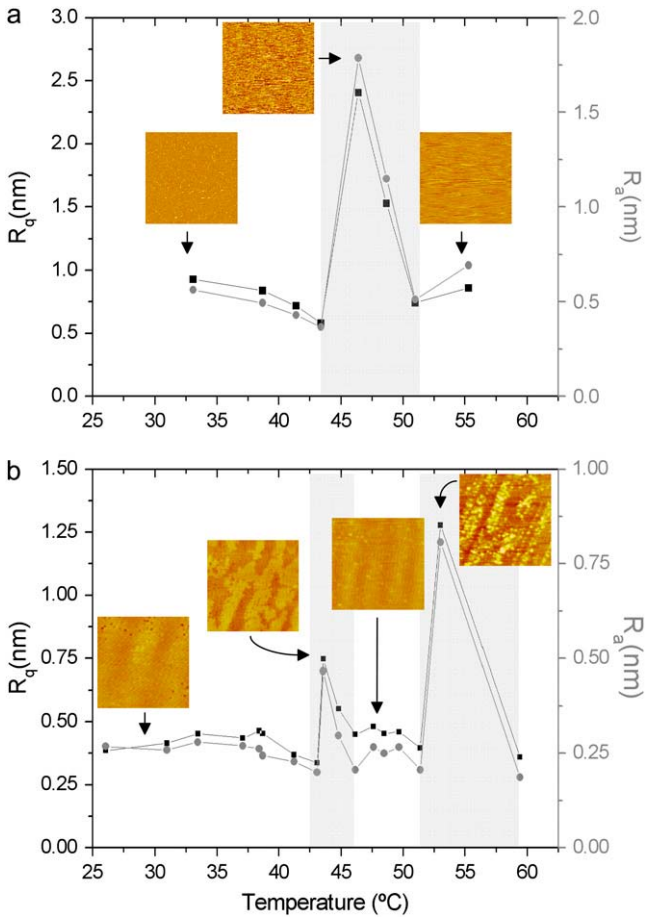

FIGURE 2 (*a*) Roughness measurements performed on the topographic images shown in Fig. 1 (DPPC monolayer). Solid line-open squares graph corresponds with R_q (*left y axis*) while shaded line-solid dots graph corresponds with R_a. The roughness increment corresponds with the LC-LE phase transition. (*b*) Roughness measurements of a series of DPPC bilayer topographic images obtained at increasing temperatures. The complete topographic series was presented in a previous work (18). The two roughness increments at ~45 and 55°C correspond with the two-phase transitions. The shaded areas in panels *a* and *b* enclose the observed transition temperature intervals. All presented images are 5 μm × 5 μm.

arisen between the bilayer and the mica surface. Other authors obtained in situ AFM evidence of two DPPC SPBs phase transitions in water. Leonenko et al. (20) reported a temperature range of 42–60°C, while Keller et al. (21) reported values from 37.8°C to 53.5°C for a mixture of DPPC and another phosphocholine. We have recently observed two transitions between 44.8°C and 59.4°C in experiments that mimic a physiological environment (18), which is also used here. Then, and assuming that the two transitions correspond to the individual melting of the two DPPC leaflets, the high temperature transition in the bilayer should correspond to the LC-LE transition of the proximal leaflet. Fig. 2 *b* shows for comparison the roughness analysis of a series of DPPC bilayer topographic images performed at variable temperature (18). Comparing the phase transition temperature intervals, marked with shaded rectangles in Fig. 2, *a* and *b*, it can be seen that the DPPC monolayer transition lies between the two transitions observed in the DPPC bilayer. Comparing the proximal leaflet transition with the monolayer transition is interesting because both the proximal leaflet and the monolayer share the same phosphocholine-mica interface but have a different medium surrounding the alkyl chain (proximal leaflet is covered by another phospholipid leaflet with alkyl chains facing downwards while the monolayer is surrounded by an aqueous solution). As shown in Fig. 1, monolayer transition occurs from 43.6 to 51.6°C, while proximal leaflet transition takes place between 52°C and 59°C (18). This fact, besides the experimental evidence of a strong coupling between the two DPPC leaflets during phase transition (19) and the roughness measurements that place the monolayer transition temperature between the two transitions observed in the bilayer, suggests that the distal monolayer stabilizes the proximal monolayer because of van der Waals interactions between the alkyl chains of the two monolayers, providing a stable, highly hydrophobic environment. Moreover, the monolayer has an unstable hydrophobic-hydrophilic interface because of the contact between the alkyl chains and the aqueous environment (48). To experimentally test the importance of the alkyl chains-medium interface in the transition temperature, several DPPC monolayers were imaged at variable temperature, but now in air. As in liquid, one transition was observed but now T_M ranged from 48°C to 51°C (three different experiments with freshly prepared samples). This implies a reduction of the transition temperature range (from 43°C to 51°C in liquid to 48–51°C in air) and also a ~4°C increase in the mean transition temperature. Air, which is more hydrophobic than an aqueous solution, stabilizes the alkyl chains of the DPPC monolayer, which translates into a T_M increase. These results experimentally prove the key role that interactions arisen in the sample interphase play in the physicochemical properties of molecularly thin structures, as is the case of DPPC monolayers.

Topography of DPPC domain edges at variable temperature imaged in air

To explore the homogeneity of the extracted LB films and to study the topographic changes at ~T_M, the same experiment presented in Fig. 1 was repeated, although this time in air conditions. Fig. 3 *a* shows a DPPC monolayer at room temperature after LB film extraction and deposition imaged by TM-AFM. This image is similar to the one obtained in aqueous buffer environment (Fig. 1 *a*), although now the presence of geometrical patterns on the monolayer is evident (some of them were marked with *solid arrows* in Fig. 3 *a* to guide the eye). As temperature was increased beyond T_M (Fig. 3 *b*), these features disappeared, yielding a flat surface. Then, the temperature was decreased to 30°C (Fig. 3 *c*) and new geometrical patterns appeared again. The presence of patterns in the LC phase and its disappearance in the LE phase suggests

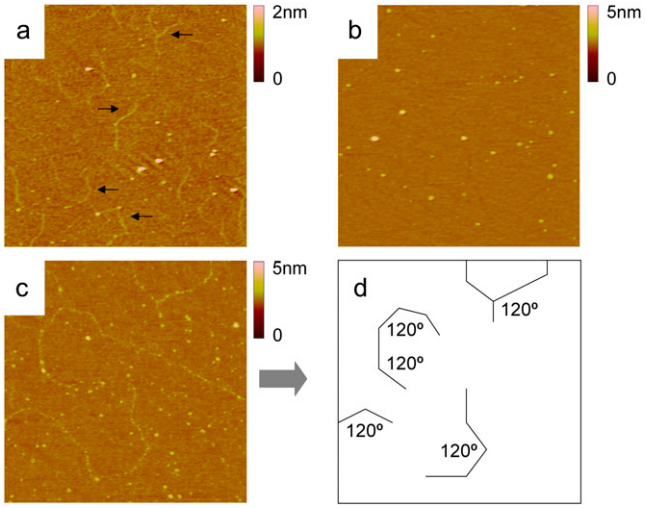

FIGURE 3 2 μm $\times$ 2 μm images of DPPC monolayers extracted at 30 mN/m and imaged in air at different temperatures. (*a*) 25°C, below T_M (LC phase); solid arrows point the presence of domain boundaries. (*b*) 65°C, above T_M (LE phase); (*c*) 30°C, below T_M (LC phase). (*d*) Scheme of the domain boundaries observed in panel *c*.

that they form part of the structure of the monolayer and that they are related to the LC-LE phase transition process. Interestingly, as the cartoon in Fig. 3 *d* shows, the patterns observed in Fig. 3 *c* form 120° angles between them. Several works have been devoted in the past to the study of domain boundaries in organic monolayers (49), phospholipid structures (44,50) and, specifically, DPPC LBs morphology has been studied during compression experiments. McConlogue (51) showed AFM images of DPPC structures on liquid subphase extracted at surface pressures ranging from 3.8 mN/m to 7.5 mN/m and corresponding to the region of LE-LC phase coexistence. As pressure increased, the LC phase domains grew at expense of the LE phase. Finally, only a film of LE phase separated the LC nuclei, which formed angles ~120° between them. As noted, the repulsive interaction between the growing LC phase nuclei can be counteracted if enough pressure is applied (52–56), which leads to the final fusion of these solid nuclei. Our results suggest that if a high enough pressure is applied (30 mN/m in our case), LC domains can merge and the domain boundaries between different nuclei are the patterns observed in Fig. 3, *a* and *c*. Indeed, hexagonal shapes were recently reported (45) during the melting of DPPC bilayers monitored by in situ AFM observations and attributed to the phospholipid intrinsic molecular packing.

To the best of our knowledge, this is the first time that domain boundaries have been imaged in a phospholipid monolayer. The structure of the domain boundary is still unclear, but it is likely to assume that it is formed by disordered DPPC molecules that were forced to occupy the mismatch between colliding LC phase domains, as it was suggested after electron diffraction measurements on phospholipid bilayers (57). In our experiments, as the temperature increases above T_M and the monolayer changes from LC to LE phase, DPPC molecules mobility increases and the domain boundaries disappear (Fig. 3 *b*). Interestingly, the presence of domain boundaries was not observed in DPPC monolayers imaged in liquid environment at any temperature, which suggests that the aqueous medium relaxes the mechanical tension formed in the domain boundaries as the monolayer is compressed from LE to LC phase (mechanical extraction process) or the phase transition from LE to LC phase takes place (temperature-controlled process). As noted before, the presence of water destabilizes the alkyl chain-medium interphase, thus reducing the phase transition temperature respective to an air interphase. Therefore, it is reasonable to think that LC phase mobility is higher in aqueous medium, leading to defect-free LC domain boundaries. An important conclusion from our findings is that the temperature-controlled solidification process undergone in temperature-controlled AFM experiments leads to the presence of domain boundaries, as well as the surface-pressure-controlled solidification process (compression in the LB trough); in both cases, a nucleation and growth of the LC phase process takes place. Future work should be done to establish the dependence of shape and size as a function of LB compression rate and cooling rate, as well as to explore the presence of domain boundaries in different polarity liquid media to discern the nature of the interphase forces responsible for the monolayer relaxation.

Force spectroscopy at variable temperature

So far, the topographic changes that the monolayer undergoes as a function of temperature have been studied. Roughness analysis of the topographic images reveals it to be a sensitive tool able to detect the main transition temperature undergone by the monolayer. However, roughness analysis provides only information about the topographic changes that take place in the surface. Rather, force spectroscopy through force-extension curves allows us to gather additional quantitative information regarding the interaction forces arisen between neighboring molecules and also to gain further insight into the mechanical properties of the monolayer with picoNewton and subnanometric resolution. The force at which the monolayer breaks, the so-called threshold force, F_y, is the maximum force that the sample is able to withstand before breaking, i.e., it marks the end of the elastic regime and the onset of the plastic deformation. In the case of lipid bilayers, we have shown that F_y is able to accurately fingerprint the bilayer phase transitions, since they involve a drastic molecular rearrangement, thus implying a change in the intermolecular interaction forces. To further understand the phase transition process in the case of the studied DPPC monolayers, we have performed multiple vertical force versus piezo displacement (FvD) curves on the monolayers, yielding experimental curves such as the one shown in Fig. 4.

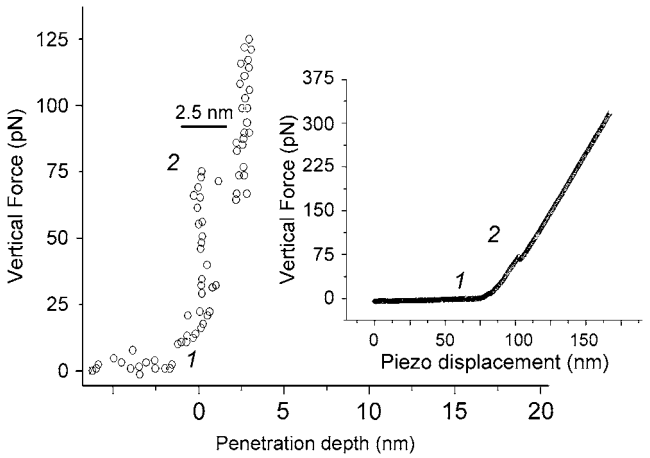

FIGURE 4 FvP curve obtained on a DPPC monolayer extracted at 30 mN/m in buffer solution at 46°C. The monolayer breakthrough can be seen at ~75 pN. (*Inset*) Corresponding FvD curve. The number *1* corresponds with the contact point and *2* is the monolayer rupture.

In this force plot, the force applied on the sample is recorded against the tip-sample distance (FvP curve). This curve is obtained from the raw force versus piezoelectric displacement curve shown in the inset as described in Materials and Methods. In each curve, the vertical force, which is proportional to the cantilever deflection, remains 0 before the contact between tip and sample, marked as point *1*. Then, vertical force increases as the tip compresses the monolayer until F_y value is reached and the tip penetrates the monolayer (point *2*). The jump in the force-penetration curve can be directly correlated with the thickness of the monolayer (55,58). The initial region of the FvP curve in Fig. 4 corresponds to the physical compression of the monolayer and to the electrostatic interaction arisen because of the slightly negative charge of the tip (56) and the weak electrical double layer promoted by the phosphocholine zwitterionic headgroups and the mica surface. Derjaguin-Landau-Verwey-Overbeek theory was applied elsewhere (16) to estimate the forces arising between a DMPC bilayer and a Si_3N_4 tip as a function of the ionic strength of the medium. Due to the low charge of the Si_3N_4 tip (0.032 C/m^2) (56), the interaction forces are in the pN range in bilayers. In the case of DPPC monolayers, interaction forces are much lower because phosphocholine polar headgroups, which are responsible for the formation of a charged interface between the membrane and the solution in bilayers, are directed toward mica in monolayers while the apolar alkyl tails, showing no dipolar moment and consequently not structuring an electric double layer, are exposed to the aqueous medium. As a result, the effect of electrostatic interactions is negligible in DPPC monolayers. Nevertheless, as the electrical double layer is practically independent of temperature for small temperature increments, F_y variation with temperature is only due to monolayer structural changes, that is, to its mechanical properties. Finally, the breakthrough event is detected as a sudden 2–3 nm penetration, which compares well with the nominal thickness of the DPPC monolayer (57) and to our scratching measurements. After penetration, the tip contacts the mica that is beneath the monolayer (13,58) and the slope of the exerted FvP curve tends to ∞.

Fig. 5 *a* shows the dependence of F_y versus temperature. FvD curves were performed from room temperature to 65°C at ~8°C intervals. Each point is the F_y average value of 150–200 individual measurements performed in several different spots on the sample surface and the error bars stand for $2\sigma/\sqrt{N}$, being σ the standard deviation and N the number of measurements (examples of the F_y histograms obtained

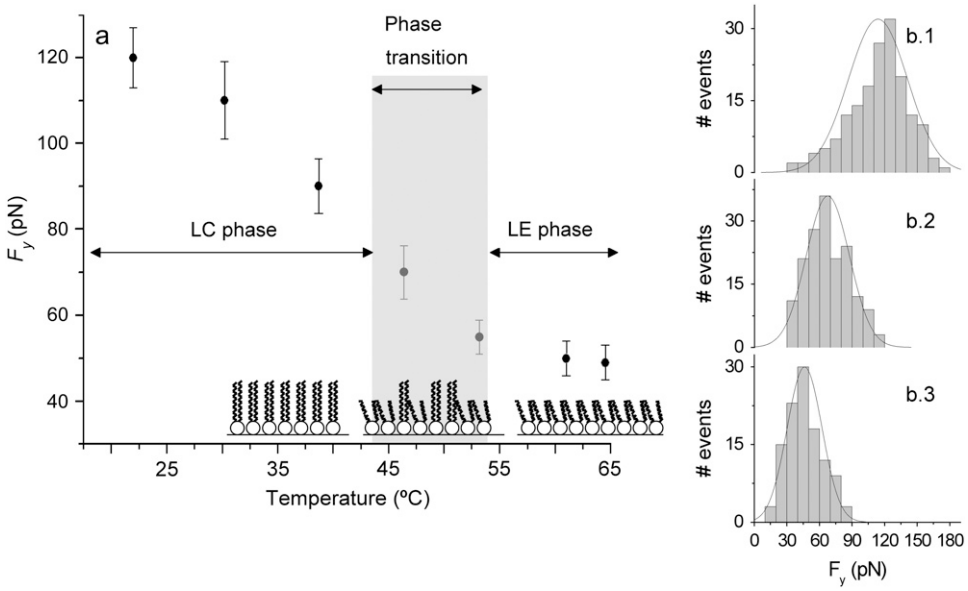

FIGURE 5 (*a*) DPPC monolayer F_y versus sample temperature. Each point is the mean value of 150–200 individual breakthrough events detected in force curves. Force curves were performed in at least four different locations for each temperature. The graph has been divided in three regions according to the monolayer phase. (*b*) Individual histograms of the experimental F_y values at different temperatures: (*b*.1) 21.2°C, (*b*.2) 46.4°C, and (*b*.3) 64.7°C.

are depicted in Fig. 5 *b*, corresponding to measurements performed at Fig. 5 *b.1*, 21.2°C; Fig. 5 *b.2*, 46.4°C; and Fig. 5 *b.3*, 67.7°C). This experiment was performed several times on different freshly prepared samples obtaining similar results. To relate F_y variations with the phase transitions detected in topographic images shown in Fig. 1, Fig. 5 *a* has been divided into three regions as in a previous work (18): LC phase, phase-transition range, and LE phase. At room temperature, F_y is 120 ± 4 pN. This force steadily decreases as temperature increases, reaching 88 ± 3 pN at 38°C near the upper temperature limit of the LC phase. During the phase transition there is a further diminution of F_y value, reaching 53 ± 2 pN at 53°C. Finally, after completing the transition, the monolayer stays in a LE phase and F_y stabilizes at ~49 ± 2 pN at 65°C.

Three important conclusions arise from these data. Firstly, F_y value is much higher in the LC phase than in the LE phase; secondly, F_y continuously decreases as temperature increases, both in the LC phase and during the transition; and thirdly, F_y ranges roughly from ~120 to ~40 pN for DPPC monolayers, while it ranges from ~25 nN to ~7 nN in DPPC bilayers in the same range of temperatures and under the same experimental conditions.

The two first conclusions are in agreement with a previous work concerning DPPC bilayers (16), where a similar trend was observed and attributed to the weakening of lateral interactions between alkane chains due to thermal energy and to the reduction of water bridges (59,60) and electrostatic interactions between polar heads during the phase transition. The weakening of lateral alkyl-alkyl interactions results in an increase in the area per molecule, that is, a decrease in the compactness of the monolayer, which translates into an increase in the molecular mobility as previously commented in Fig. 2 (61), where LC phase roughness decreases before reaching the phase transition.

Consequently, the weakening of lateral interactions between molecules translates into a F_y reduction. Different factors account for the notorious difference in mechanical properties between DPPC monolayers and bilayers; first of all, the monolayers expose the hydrophobic alkyl chains toward the aqueous solution. It has been experimentally demonstrated that the interactions between water-alkyl chains are 10 times weaker than the interaction between water molecules (48), leading to an interphase that destabilizes the monoayer. Conversely, the bilayer exposes the polar zwitterionic headgroups toward the solution, which is a favorable interaction in terms of hydrophilicity. Ions also play an important role stabilizing phosphocholine heads (16), as has been studied by molecular dynamics, concluding that up to three phosphate moieties can be coordinated by each Na^+ ion (17). Additional experimental observations concluded that the self-diffusion of 1-palmitoyl-2-oleoylphosphatidylcholine decreases due to the presence of NaCl in the medium (62) and that polar headgroups orientation is also perturbed (63), which confirms the key role that free charges play in the stability of bilayers. Another factor that improves bilayer cohesion is the hydrophobic interaction between the alkyl chains of the two leaflets, as detected in studying lipid diffusivity by means of fluorescence techniques (64). Nevertheless, this can be a minor issue in the stability of the bilayer, as lipid diffusion studies concerning DPPC bilayers (52) suggest that the hydrophobic interactions between the two lipid leaflets are weaker than the interactions between the lower leaflet and the (silica) substrate.

To relate the DPPC monolayer structure with the measured F_y values, different interactions should be considered, namely electrostatic and van der Waals forces. Because of the mica surface negative charge (53) and the positive charge of the choline headgroups (phosphocholine is a zwitterionic headgroup with the choline positive charge facing toward the mica surface), electrostatic interactions arise. Nevertheless, it was observed by several techniques such as neutron reflectivity (65,66) and fluorescence interference-contrast microscopy (67,68) that there is a sandwiched water layer with a thickness ranging from 10 to 30 Å between the substrate and the phospholipid bilayers. Related experiments concerning the effect of pH and ionic strength in bilayer spreading on oxides revealed that the equilibrium distance between the polar heads and the substrate surface is ~1 nm (69) and that this gap is full of water molecules. Although there is some controversy about the level of water organization forced by the substrate (70), the presence of structured water on the surface of mica and silica was proved by scanning polarization force microscopy, sum-frequency-generation vibrational spectroscopy (71), and Monte Carlo simulations (72). As a consequence, the water layer between the substrate and the DPPC polar headgroups provides fluidity and mobility to the bilayer (3,45,69). As a first approximation and due to the screening effect of the water sandwiched underneath the monolayer, electrostatic interactions between mica and DPPC polar heads have been neglected in this study.

The electrostatic interactions arisen between polar headgroups have been discussed in several simulation works, suggesting that ions can penetrate the polar headgroups to screen the charges of the choline and phosphate moieties (17,62,63,73). Nevertheless, as the calculation of these electrostatic interactions is out of the scope of this work and for the sake of simplicity, van der Waals forces between hydrocarbon chains will be considered as the most representative interaction between DPPC molecules.

The van der Waals interaction between hydrocarbon chains (E_{VdW}) can be expressed as (71)

$$E_{VdW} = \frac{3\alpha_0^2 h\nu}{4(4\pi\varepsilon_0)^2}\left[\frac{6}{\sigma^2} + \frac{12}{[\sigma^2 + l^2]^3} + \frac{12}{[\sigma^2 + (2l)^2]^3} + \ldots\right]\frac{N_0}{2}, \quad (3)$$

with α_o being the polarizability, ε_o the vacuum permittivity, σ the distance between two equivalent $-CH_2$ groups in adjacent molecules, l the distance between consecutive

$-CH_2$ groups in the same hydrocarbon chain, and N_o Avogadro's number. As the monolayer was extracted at 30 mN/m, the area/DPPC molecule is 54.7 Å^2 in a hexagonal lattice (36,45,74–76). As each DPPC molecule has two hydrocarbon chains, it has been considered that each chain occupies an area equal to 54.7/2 Å^2. Circles in Fig. 6 *a* correspond to the molecular DPPC area in the monolayer and the solid dots represent the hydrocarbon chains seen from above, while Fig. 6 *b* shows a side view of the same structure. The alignment of the chains in the *y* direction correspond to the packing optimization of van der Waals interactions, which has been mostly studied in alkanethiols (77–79) and alkanesilanes (80). Van der Waals forces considered in this study include the interactions between a $-CH_2$ group and the six adjacent $-CH_2$ groups in the same plane and also the interaction with the $-CH_2$ groups that are one and two planes higher and lower. This interaction was multiplied by a factor of 2 because there are two chains in each molecule. The interactions between $-CH_2$ groups in the same molecule were not considered because only intermolecular energies are to be estimated. The resulting energy was multiplied by 16, which is the length of the DPPC hydrocarbon chains, obtaining $E_{VdW} = 19.4$ KJ/mol.

The experimental energy needed to puncture the monolayer during force spectroscopy measurements (E) can be calculated as

$$E = F_y * \delta. \tag{4}$$

At room temperature, DPPC monolayer F_y is 120 ± 4 pN and δ is 2.4 nm (36,37), so E is 0.29 10^{-18} J. Although this energy is mainly consumed in the monolayer breakthrough process, part of it is possibly dissipated through nonconservative processes such as viscous damping or hysteresis effects (81). Energy dissipation was measured in dynamic force microscopy experiments concerning different kinds of surfaces and tip configurations, yielding values in the eV range (82). As a consequence, it is reasonable to think that, in force spectroscopy experiments, similar processes will take place. Nevertheless, and due to the semiquantitative nature of the energetic calculations proposed in this work, energy dissipation has not been accounted for.

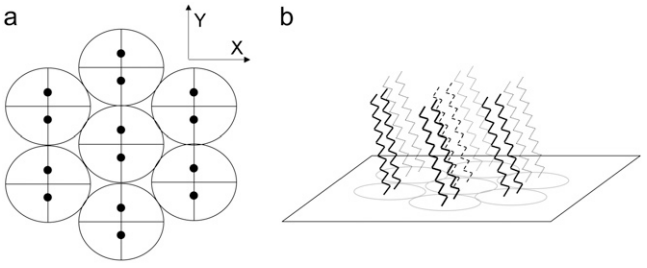

FIGURE 6 (*a*) Upper view of the DPPC hexagonal packing. The circles represent the DPPC molecular area and the solid dots represent the hydrocarbon chains. (*b*) Lateral view of the same structure. The DPPC hydrocarbon chains are tilted 25° when no vertical load is applied.

To estimate the contact area between tip and monolayer and the number of molecules affected by the tip during spectroscopy experiments, a Hertz contact model has been applied. In a previous work (16), we demonstrated that a contact mechanics model based on the coupling of n springs is more realistic than a Hertz model when it comes to explain the elastic region of a phospholipid bilayer before indentation (83). Nevertheless, and to calculate the contact area between tip and sample at low loads, a Hertz model is accurate enough because it does not consider long-range forces arisen between tip and sample, which is the case of our experiments, as no jump to contact was detected in FvD curves (Fig. 4) The Hertzian contact area (A) is expressed as

$$A = \pi(RF/K)^{2/3}, \tag{5}$$

where R is the tip radius, F is the vertical force and K is the combined elastic moduli

$$K = 4/3\left((1-\nu_1^2)/E_1 + (1-\nu_2^2)/E_2\right)^{-1}, \tag{6}$$

where ν_1 and ν_2 are the Poisson ratios of the tip and the sample, 0.2 (84) and 0.5, respectively (14,85), and E_1 and E_2 are the Young's moduli of the tip and the sample, 280 GPa (84) and 15 MPa (86). Considering the experimental area/DPPC molecule and $F_y = 120$ pN, the number of affected molecules is ~205 for $R = 15$ nm and ~360 for $R = 35$ nm. These R values are the maximum and minimum tip radius measured in the presented experiments and can be considered as typical upper and lower limits for the vast majority of force spectroscopy studies. Dividing the total applied energy during the breakthrough process by the number of affected molecules, a breakthrough energy (E_b) of 0.8 KJ/mol for R_{15nm} and 0.5 KJ/mol for R_{35nm} is obtained. It was previously shown that the E_{VdW} is 19.4 KJ/mol, an order-of-magnitude bigger than E_b. This fact seems to suggest that the energy necessary to break the DPPC monolayer is 20–40 times lower than the van der Waals interaction between all the hydrocarbon chains of the molecules in the penetration-affected area. Regarding these results, it is reasonable to think that, to puncture the monolayer, it is not necessary to break all the interactions between all the molecules but only a fraction of them, so E_b should be lower than E_{VdW}. As an attempt to explain how the monolayer reacts to the pressure, Fig. 7 shows two possible monolayer rupture mechanisms. Fig. 7 *a* represents an upper view of the hexagonal DPPC lattice and a circle that encloses the Hertzian area of contact between the tip and the sample. The simplest rupture model proposed is a straight line (*dotted line* in Fig. 7, *a* and *b*). Possibly, the presence of a vacancy or any defect in the structure would be the starting point of the monolayer rupture process. The fragile nature of phospholipid structures has been suggested before (16,87), mainly because of the kind of breakthrough seen in force spectroscopy experiments, which always implies a sudden penetration, more similar to a fragile brittle fracture than to the compression

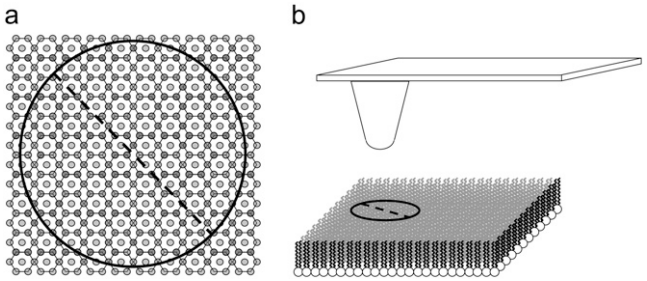

FIGURE 7 (*a*) Upper view of a DPPC monolayer hexagonal packing. The solid circle encloses the Hertzian contact area during a penetration experiment. Two monolayer rupture models are proposed in this work: across a straight line (*dotted line*) and across the perimeter of the Hertzian contact area. (*b*) Lateral view of the same structure.

of a soft material. The breakthrough event in the FvP curve shown in Fig. 4 occurs at a certain F_y and it is a sudden all-or-none process, as the tip penetrates the monolayer in a one-step mechanism. Another possibility would be a monolayer failure along the contact area perimeter (*circle* in Fig. 7, *a* and *b*). Both the linear and perimeter rupture imply the disruption of a certain number of van der Waals interactions, which depends on the contact area. Concerning the number of alkyl chain interactions broken during penetration, these models can be considered as extreme possibilities, so the real process is possibly a combination of both. Table 1 summarizes the percentage of van der Waals interactions broken in the linear ($\%R_l$) and circular model ($\%R_p$) with respect to the total number of van der Waals interactions present in the whole contact area. Depending on the rupture model and R, $\%R_l$ and $\%R_p$ range from 5 to 16%, so this percentage is an estimation of the van der Waals interactions broken during the penetration process respective to the total number of van der Waals interactions. Table 1 also shows the relationship between E_b and E_{VdW}, which is the ratio between the energy used to break the monolayer and the total van der Waals interactions between the hydrocarbon chains ($\%(E_b/E_{VdW})$). This ratio ranges from 3 to 4%. The similarity between the ratios $\%R_l$, $\%R_p$, and $\%(E_b/E_{VdW})$ suggests that the linear and circular models are consistent with experimental data. As a consequence, it can be considered that, although several forces are involved in the cohesion of DPPC monolayers, interchain van der Waals interactions play a key role in the mechanical properties of DPPC monolayers and that electrostatic interactions between polar heads and between choline groups and mica surface can be neglected as a first approximation. Of course, the nature of the calculations presented in this work can not discriminate between the two proposed models but it provides a framework to study the behavior of phospholipid monolayers under compression. Further studies exploring the effect of different polar heads and different alkyl chains length will provide a deeper insight in the effect that electrostatic and van der Waals forces play in the cohesion and mechanical response of phospholipid monolayers and bilayers.

TABLE 1 Mechanical and structural parameters of a DPPC monolayer compressed by an AFM tip of radius 15 nm and 35 nm

	$R = 15$ nm	$R = 35$ nm
Affected molecules (Hertz model)	205	360
E_b (Kj/mol)	0.8	0.5
% Broken van der Waals interactions in a linear rupture ($\%R_l$)	5	4
% Broken van der Waals interactions in a circular rupture ($\%R_p$)	16	11
$\%(E_b/E_{VdW})$	4	3

CONCLUSIONS

Langmuir-Blodgett DPPC monolayers extracted at 30 mN/m were imaged in situ by variable temperature TM-AFM. The experiments performed in buffer environment revealed that only one phase transition takes place at $\sim T_M$, which suggests that the two transitions observed in DPPC bilayers in the same buffer media correspond to the melting of the two separate phospholipid leaflets. DPPC monolayer T_M lies between the two transitions observed in DPPC bilayers. We propose that the monolayer can be compared to the leaflet in contact with the substrate in the bilayer structure (high temperature transition) but destabilized by the water-alkyl chains interphase and the lack of the stabilizing hydrophobic interaction between the alkyl chains of the two phospholipid leaflets that form the bilayer. DPPC monolayer T_M increases in air, where a favorable air-alkyl chains interphase arises, which further supports this conclusion. The topographic study of DPPC monolayers imaged in air revealed the presence of 120° LC phase domain boundaries both created during the mechanical compression in the LB trough and during the cooling from LE to LC phase. The boundaries disappear above T_M and are recovered if the sample is cooled again to room temperature, suggesting that a nucleation and growth mechanism is responsible for the formation of the LC phase when cooling from the LE phase.

The mechanical study by force spectroscopy showed F_y values in the pN range for DPPC monolayers, two orders-of-magnitude lower than those obtained in DPPC bilayers. Nevertheless, the overall trend of monolayers and bilayers is similar upon raising temperature: In the solid phase, F_y decreases as temperature increases, while it stabilizes at a lower value in the liquid phase. To relate F_y values with DPPC monolayers structure, a simple geometric model concerning van der Waals interactions between the phospholipid alkane chains has been proposed. Applying Hertz contact mechanics, the energy/DPPC molecule applied on the monolayer during penetration experiments was calculated and assuming simple models for the monolayer rupture (namely across a straight line or around the perimeter of the contact area

between tip and sample), a good accordance between the experimental data and the geometric model was found.

This work paves the way for more complex studies involving mixed monolayers systems, where temperature-controlled AFM imaging could shed light on the different transition processes that monolayers (and bilayers) undergo when mixing miscible or immiscible phospholipid molecules. Besides, force spectroscopy proves to be a suitable technique to identify different phospholipid phases, as F_y value is highly dependent on the phospholipid structure, and can be used to explore the different intermolecular interactions arisen in biological membranes.

G.O. and L.P. are recipients of a ''Recerca i Docència'' fellowship from the University of Barcelona.

This work was supported by grant No. CTQ2004-08046 from Ministerio de Ciencia y Tecnología and grant No. SGR00664 from Generalitat de Catalunya of Spain.

REFERENCES

1. Vogel, V., and M. Sheetz. 1983. Local force and geometry sensing regulate cell functions. *Nature Rev.* 7:265–275.
2. Sheetz, M. P., J. E. Sable, and H. G. Dobereiner. 2006. Continuous membrane-cytoskeleton adhesion requires continuous accommodation to lipid and cytoskeleton dynamics. *Annu. Rev. Biophys. Biomol. Struct.* 35:417–434.
3. Sackmann, E. 1996. Supported membranes: scientific and practical applications. *Science.* 271:43–48.
4. Heimburg, T. 1998. Mechanical aspects of membrane thermodynamics. estimation of the mechanical properties of lipid membranes close to the chain melting transition from calorimetry. *Biochim. Biophys. Acta.* 1415: 147–162.
5. Lee, C. H., W. C. Lin, and J. Wang. 2001. All-optical measurements of the bending rigidity of lipid-vesicle membranes across structural phase transitions. *Phys. Rev. E Stat. Nonlin. Soft Matter Phys.* 64:020901.
6. Dimova, R., B. Pouligny, and C. Dietrich. 2000. Pretransitional effects in dimyristoylphosphatidylcholine vesicle membranes: optical dynamometry study. *Biophys. J.* 79:340–356.
7. Evans, E., and D. Needham. 1987. Physical properties of surfactant bilayer membranes—thermal transitions, elasticity, rigidity, cohesion, and colloidal interactions. *J. Phys. Chem.* 91:4219–4228.
8. Meleard, P., C. Gerbeaud, P. Bardusco, N. Jeandaine, M. D. Mitov, and L. Fernandez-Puente. 1998. Mechanical properties of model membranes studied from shape transformations of giant vesicles. *Biochimie.* 80:401–413.
9. Mueller, H., H. J. Butt, and E. Bamberg. 1999. Force measurements on myelin basic protein adsorbed to mica and lipid bilayer surfaces done with the atomic force microscope. *Biophys. J.* 76:1072–1079.
10. Zasadzinski, J. A., C. A. Helm, M. L. Longo, A. L. Weisenhorn, S. A. Gould, and P. K. Hansma. 1991. Atomic force microscopy of hydrated phosphatidylethanolamine bilayers. *Biophys. J.* 59:755–760.
11. Egger, M., F. Ohnesorge, A. L. Weisenhorn, S. P. Heyn, B. Drake, C. B. Prater, S. A. C. Gould, P. K. Hansma, and H. E. Gaub. 1990. Wet lipid protein membranes imaged at submolecular resolution by atomic force microscopy. *J. Struct. Biol.* 103:89–94.
12. Garcia-Manyes, S., G. Oncins, and F. Sanz. 2006. Effect of pH and ionic strength on phospholipid nanomechanics and on deposition process onto hydrophilic surfaces measured by atomic force microscopy. *Electrochim. Acta.* 51:5029–5036.
13. Franz, V., S. Loi, H. Muller, E. Bamberg, and H. H. Butt. 2002. Tip penetration through lipid bilayers in atomic force microscopy. *Colloids Surf. B.* 23:191–200.
14. Kunneke, S., D. Kruger, and A. Janshoff. 2004. Scrutiny of the failure of lipid membranes as a function of headgroups, chain length, and lamellarity measured by scanning force microscopy. *Biophys. J.* 86: 1545–1553.
15. Liang, X. M., G. Z. Mao, and K. Y. S. Ng. 2004. Probing small unilamellar EggPC vesicles on mica surface by atomic force microscopy. *Colloids Surf. B.* 34:41–51.
16. Garcia-Manyes, S., G. Oncins, and F. Sanz. 2005. Effect of ion-binding and chemical phospholipid structure on the nanomechanics of lipid bilayers studied by force spectroscopy. *Biophys. J.* 89:1812–1826.
17. Bockmann, R. A., A. Hac, T. Heimburg, and H. Grubmuller. 2003. Effect of sodium chloride on a lipid bilayer. *Biophys. J.* 85:1647–1655.
18. Garcia-Manyes, S., G. Oncins, and F. Sanz. 2005. Effect of temperature on the nanomechanics of lipid bilayers studied by force spectroscopy. *Biophys. J.* 89:4261–4274.
19. Yang, J., and J. Appleyard. 2000. The main phase transition of mica-supported phosphatidylcholine membranes. *J. Phys. Chem. B.* 104: 8097–8100.
20. Leonenko, Z. V., E. Finot, H. Ma, T. E. Dahms, and D. T. Cramb. 2004. Investigation of temperature-induced phase transitions in DOPC and DPPC phospholipid bilayers using temperature-controlled scanning force microscopy. *Biophys. J.* 86:3783–3793.
21. Keller, D., N. B. Larsen, I. M. Moller, and O. G. Mouritsen. 2005. Decoupled phase transitions and grain-boundary melting in supported phospholipid bilayers. *Phys. Rev. Lett.* 94:025701.
22. Bonnerot, A., P. A. Chollet, H. Frisby, and M. Hoclet. 1985. Infrared and electron-diffraction studies of transient stages in very thin Langmuir-Blodgett films. *Chem. Phys.* 97:365–377.
23. Bohm, C., R. Steitz, and H. Riegler. 1989. Temperature-dependent electron-diffraction studies of cadmium arachidate monolayers and multilayers. *Thin Solid Films.* 178:511–517.
24. Peterson, I. R., R. Steitz, H. Krug, and I. Voigtmartin. 1990. An investigation of the spot profiles in transmission electron-diffraction from Langmuir-Blodgett films of aliphatic chain compounds. *J. Phys. [E].* 51:1003–1026.
25. Rabe, J. P., J. D. Swalen, and J. F. Rabolt. 1987. Order-disorder transitions in Langmuir-Blodgett films. 3. Polarized Raman studies of cadmium arachidate using integrated optical techniques. *J. Chem. Phys.* 86:1601–1607.
26. Nakanaga, T., M. Matsumoto, Y. Kawabata, H. Takeo, and C. Matsumura. 1989. Observation of FTIR-PA spectra of Langmuir-Blodgett films of cadmium arachidate on glass plates. *Chem. Phys. Lett.* 160:129–133.
27. Nag, K., C. Boland, N. Rich, and K. M. Keough. 1991. Epifluorescence microscopic observation of monolayers of dipalmitoylphosphatidylcholine: dependence of domain size on compression rates. *Biochim. Biophys. Acta.* 1068:157–160.
28. Schwartz, D. K., J. Garnaes, R. Viswanathan, and J. A. N. Zasadzinski. 1992. Surface order and stability of Langmuir-Blodgett films. *Science.* 257:508–511.
29. Schwartz, D. K., R. Viswanathan, J. Garnaes, and J. A. Zasadzinski. 1993. Influence of cations, alkane chain-length, and substrate on molecular order of Langmuir-Blodgett films. *J. Am. Chem. Soc.* 115:7374–7380.
30. Viswanathan, R., L. L. Madsen, J. A. Zasadzinski, and D. K. Schwartz. 1995. Liquid to hexatic to crystalline order in Langmuir-Blodgett films. *Science.* 269:51–54.
31. Bourdieu, L., O. Ronsin, and D. Chatenay. 1993. Molecular positional order in Langmuir-Blodgett films by atomic force microscopy. *Science.* 259:798–801.
32. Zhai, X., and J. M. Kleijn. 1997. Molecular structure of dipalmitoylphosphatidylcholine Langmuir-Blodgett monolayers studied by atomic force microscopy. *Thin Solid Films.* 304:327–332.
33. Florin, E. L., M. Rief, H. Lehmann, M. Ludwig, C. Dornmair, V. T. Moy, and H. E. Gaub. 1995. Sensing specific molecular-interactions with the atomic-force microscope. *Biosens. Bioelectron.* 10:895–901.

34. Proksch, R., T. E. Schaffer, J. P. Cleveland, R. C. Callahan, and M. B. Viani. 2004. Finite optical spot size and position corrections in thermal spring constant calibration. *Nanotechnology*. 15:1344–1350.

35. Cevc, G., and D. Marsh. 1987. Phospholipid Bilayers. Physical Principles and Models. Wiley-Interscience, New York.

36. Chunbo, Y., D. Desheng, L. Zuhong, and L. Juzheng. 1999. Molecular positional order in a dipalmitoylphosphatidic acid Langmuir-Blodgett monolayer by atomic force microscopy. *Colloids Surf. A*. 150:1–6.

37. Greenhall, M. H., P. J. Lukes, M. C. Petty, J. Yarwood, and Y. Lvov. 1994. The formation and characterization of Langmuir-Blodgett films of dipalmitoylphosphatidic acid. *Thin Solid Films*. 243:596–601.

38. Huang, C. H., and S. S. Li. 1999. Calorimetric and molecular mechanics studies of the thermotropic phase behavior of membrane phospholipids. *Biochim. Biophys. Acta*. 1422:273–307.

39. Watry, M. R., T. L. Tarbuck, and G. I. Richmond. 2003. Vibrational sum-frequency studies of a series of phospholipid monolayers and the associated water structure at the vapor. *J. Phys. Chem. B*. 107: 512–518.

40. Jyoti, A., R. M. Prokop, J. Li, D. Vollhardt, D. Y. Kwok, R. Miller, H. Mohwald, and A. W. Neumann. 1996. An investigation of the compression rate dependence on the surface pressure-surface area isotherm for a dipalmitoyl phosphatidylcholine monolayer at the air. *Colloids Surf. A*. 116:173–180.

41. Lalchev, Z. I., and A. R. Mackie. 1999. Molecular lateral diffusion in model membrane systems. *Colloids Surf. B*. 15:147–160.

42. Mingins, J., D. Stigter, and K. A. Dill. 1992. Phospholipid interactions in model membrane systems. I. Experiments on monolayers. *Biophys. J*. 61:1603–1615.

43. Stigter, D., J. Mingins, and K. A. Dill. 1992. Phospholipid interactions in model membrane systems. II. Theory. *Biophys. J*. 61:1616–1629.

44. Heimburg, T. 2000. A model for the lipid pretransition: coupling of ripple formation with the chain-melting transition. *Biophys. J*. 78:1154–1165.

45. Feng, Z. V., T. A. Spurlin, and A. A. Gewirth. 2005. Direct visualization of asymmetric behavior in supported lipid bilayers at the gel-fluid phase transition. *Biophys. J*. 88:2154–2164.

46. Charrier, A., and F. Thibaudau. 2005. Main phase transitions in supported lipid single-bilayer. *Biophys. J*. 89:1094–1101.

47. Ma, G., and H. C. Allen. 2006. DPPC Langmuir monolayer at the air-water interface: probing the tail and head groups by vibrational sum frequency generation spectroscopy. *Langmuir*. 22:5341–5349.

48. Gunster, J., and R. Souda. 2006. On the wettability of lipid DPPC films. *Langmuir*. 22:6939–6943.

49. Last, J. A., A. C. Hillier, D. E. Hooks, J. B. Maxson, and M. D. Ward. 1998. Epitaxially driven assembly of crystalline molecular films on ordered substrates. *Chem. Mater*. 10:422–437.

50. Schneider, M. F., D. Marsh, W. Jahn, B. Kloesgen, and T. Heimburg. 1999. Network formation of lipid membranes: triggering structural transitions by chain melting. *Proc. Natl. Acad. Sci. USA*. 96:14312–14317.

51. McConlogue, C. W., and T. K. Vanderlick. 1997. A close look at domain formation in DPPC monolayers. *Langmuir*. 13:7158–7164.

52. Hetzer, M., S. Heinz, S. Grage, and T. M. Bayerl. 1998. Asymmetric molecular friction in supported phospholipid bilayers revealed by NMR measurements of lipid diffusion. *Langmuir*. 14:982–984.

53. Nishimura, S., S. Biggs, P. J. Scales, T. W. Healy, K. Tsunematsu, and T. Tateyama. 1994. Molecular-scale structure of the cation modified muscovite mica basal-plane. *Langmuir*. 10:4554–4559.

54. Garcia-Manyes, S., O. Domènech, F. Sanz, M. T. Montero, and J. Hernandez-Borrell. 2007. Atomic force microscopy and force spectroscopy study of Langmuir-Blodgett films formed by heteroacid phospholipids of biological interest. *Biochim. Biophys. Acta*. Accepted.

55. Schneider, J., Y. F. Dufrene, W. R. Barger, and G. U. Lee. 2000. Atomic force microscope image contrast mechanisms on supported lipid bilayers. *Biophys. J*. 79:1107–1118.

56. Butt, H. J. 1991. Measuring electrostatic, van der Waals, and hydration forces in electrolyte solutions with an atomic force microscope. *Biophys. J*. 60:1438–1444.

57. Yang, X. M., D. Xiao, S. J. Xiao, and Y. Wei. 1994. Domain structures of phospholipid monolayer Langmuir-Blodgett films determined by atomic-force microscopy. *Appl. Phys. Mater. Sci. Process*. 59:139–143.

58. Schneider, J., W. Barger, and G. U. Lee. 2003. Nanometer scale surface properties of supported lipid bilayers measured with hydrophobic and hydrophilic atomic force microscope probes. *Langmuir*. 19:1899–1907.

59. Pasenkiewicz-Gierula, M., Y. Takaoka, H. Miyagawa, K. Kitamura, and A. Kusumi. 1999. Charge pairing of headgroups in phosphatidylcholine membranes: a molecular dynamics simulation study. *Biophys. J*. 76:1228–1240.

60. Pasenkiewicz-Gierula, M., Y. Takaoka, H. Miyagawa, K. Kitamura, and A. Kusumi. 1997. Hydrogen bonding of water to phosphatidylcholine in the membrane as studied by a molecular dynamics simulation: location, geometry, and lipid-lipid bridging via hydrogen-bonded water. *J. Phys. Chem. A*. 101:3677–3691.

61. Lindblom, G., G. Oradd, and A. Filippov. 2006. Lipid lateral diffusion in bilayers with phosphatidylcholine, sphingomyelin and cholesterol—an NMR study of dynamics and lateral phase separation. *Chem. Phys. Lipids*. 141:179–184.

62. Bockmann, R. A., and H. Grubmuller. 2004. Multistep binding of divalent cations to phospholipid bilayers: a molecular dynamics study. *Angew. Chem. Int. Ed. Engl*. 43:1021–1024.

63. Sachs, J. N., H. Nanda, H. I. Petrache, and T. B. Woolf. 2004. Changes in phosphatidylcholine headgroup tilt and water order induced by monovalent salts: molecular dynamics simulations. *Biophys. J*. 86:3772–3782.

64. Merkel, R., E. Sackmann, and E. Evans. 1989. Molecular friction and epitactic coupling between monolayers in supported bilayers. *J. Phys. [E]*. 50:1535–1555.

65. Johnson, S. J., T. M. Bayerl, D. C. McDermott, G. W. Adam, A. R. Rennie, R. K. Thomas, and E. Sackmann. 1991. Structure of an adsorbed dimyristoylphosphatidylcholine bilayer measured with specular reflection of neutrons. *Biophys. J*. 59:289–294.

66. Koenig, B. W., S. Kruger, W. J. Orts, C. F. Majkrzak, N. F. Berk, J. V. Silverton, and K. Gawrisch. 1996. Neutron reflectivity and atomic force microscopy studies of a lipid bilayer in water adsorbed to the surface of a silicon single crystal. *Langmuir*. 12:1343–1350.

67. Kiessling, V., and L. K. Tamm. 2003. Measuring distances in supported bilayers by fluorescence interference-contrast microscopy: polymer supports and SNARE proteins. *Biophys. J*. 84:408–418.

68. Fromherz, P., V. Kiessling, K. Kottig, and G. Zeck. 1999. Membrane transistor with giant lipid vesicle touching a silicon chip. *Appl. Phys. Mater. Sci. Process*. 69:571–576.

69. Cremer, P. S., and S. G. Boxer. 1999. Formation and spreading of lipid bilayers on planar glass supports. *J. Phys. Chem. B*. 103:2554–2559.

70. Kim, J., G. Kim, and P. S. Cremer. 2001. Investigations of water structure at the solid. *Langmuir*. 17:7255–7260.

71. Miranda, P. B., L. Xu, Y. R. Shen, and M. Salmeron. 1998. Icelike water monolayer adsorbed on mica at room temperature. *Phys. Rev. Lett*. 81:5876–5879.

72. Park, S. H., and G. Sposito. 2002. Structure of water adsorbed on a mica surface. *Phys. Rev. Lett*. 89:085501.

73. Pandit, S. A., D. Bostick, and M. L. Berkowitz. 2003. Molecular dynamics simulation of a dipalmitoylphosphatidylcholine bilayer with NaCl. *Biophys. J*. 84:3743–3750.

74. Israelachvili, J. 1992. Intermolecular and Surface Forces. Academic Press, San Diego, CA.

75. Hui, S. W., D. F. Parsons, and M. Cowden. 1974. Electron-diffraction of wet phospholipid bilayers. *Proc. Natl. Acad. Sci. USA*. 71:5068–5072.

76. Janiak, M. J., D. M. Small, and G. G. Shipley. 1979. Temperature and compositional dependence of the structure of hydrated dimyristoyl lecithin. *J. Biol. Chem*. 254:6068–6078.

77. Ulman, A., J. E. Eilers, and N. Tillman. 1989. Packing and molecular-orientation of alkanethiol monolayers on gold surfaces. *Langmuir*. 5:1147–1152.

78. Barrena, E., C. Ocal, and M. Salmeron. 2000. Molecular packing changes of alkanethiols monolayers on Au_{11} under applied pressure. *J. Chem. Phys.* 113:2413–2418.

79. Barrena, E., C. Ocal, and M. Salmeron. 2001. Structure and stability of tilted-chain phases of alkanethiols on Au_{11}. *J. Chem. Phys.* 114:4210–4214.

80. Barrena, E., S. Kopta, D. F. Ogletree, D. H. Charych, and M. Salmeron. 1999. Relationship between friction and molecular structure: alkylsilane lubricant films under pressure. *Phys. Rev. Lett.* 82:2880–2883.

81. Schirmeisen, A., and H. Holscher. 2005. Velocity dependence of energy dissipation in dynamic force microscopy: hysteresis versus viscous damping. *Phys. Rev. B*. 72:045431.

82. Garcia, R., C. J. Gomez, N. F. Martinez, S. Patil, C. Dietz, and R. Magerle. 2006. Identification of nanoscale dissipation processes by dynamic atomic force microscopy. *Phys. Rev. Lett.* 97:016103.

83. Fraxedas, J., S. Garcia-Manyes, P. Gorostiza, and F. Sanz. 2002. Nanoindentation: toward the sensing of atomic interactions. *Proc. Natl. Acad. Sci. USA*. 99:5228–5232.

84. Khan, A., J. Philip, and P. Hess. 2004. Young's modulus of silicon nitride used in scanning force microscope cantilevers. *J. Appl. Phys.* 95:1667–1672.

85. Voitchovsky, K., S. Antoranz Contera, M. Kamihira, A. Watts, and J. F. Ryan. 2006. Differential stiffness and lipid mobility in the leaflets of purple membranes. *Biophys. J.* 90:2075–2085.

86. Hantz, E., A. Cao, J. Escaig, and E. Taillandier. 1986. The osmotic response of large unilamellar vesicles studied by quasi-elastic light scattering. *Biochim. Biophys. Acta*. 862:379–386.

87. Oncins, G., S. Garcia-Manyes, and F. Sanz. 2005. Study of frictional properties of a phospholipid bilayer in a liquid environment with lateral force microscopy as a function of NaCl concentration. *Langmuir*. 21:7373–7379.